Data in Brief 52 (2024) 109971

Contents lists available at ScienceDirect

Data in Brief

journal homepage: www.elsevier.com/locate/dib

Data Article

Dataset on density functional theory investigation of ternary Heusler alloys

Ridwan Nahar, Ka Ming Law, Thomas Roden, Michael Zengel, Justin Lewis, Sujan Budhathoki, Riley Nold, Harshil Avlani, Babajide Akintunde, Naomi Derksen, Adam J. Hauser*

Department of Physics and Astronomy, University of Alabama, AL, United States

ARTICLE INFO

Article history:
Received 1 October 2023
Revised 8 December 2023
Accepted 13 December 2023
Available online 18 December 2023

Dataset link: Dataset on Density Functional Theory investigation of Ternary Heusler Alloys (Original data)

Keywords:
Density functional theory (DFT)
Heusler alloys
Formation energy
Magnetic moment
Spin polarization
Density of states
Projected density of states

ABSTRACT

This paper contains data and results from Density Functional Theory (DFT) investigation of 423 distinct X_2YZ ternary full Heusler alloys, where X and Y represent elements from the D-block of the periodic table and Z signifies element from main group. The study encompasses both "regular" and "inverse" Heusler phases of these alloys for a total of 846 potential materials. For each specific alloy and each phase, a range of information is provided including total energy, formation energy, lattice constant, total and site-specific magnetic moments, spin polarization as well as total and projected density of electronic states. The aim of creating this dataset is to provide fundamental theoretical insights into ternary X_2YZ Heusler alloys for further theoretical and experimental analysis.

* Corresponding author.
E-mail address: ahauser@ua.edu (A.J. Hauser).

https://doi.org/10.1016/j.dib.2023.109971

Specification Table

Subject	Condensed Matter Physics
Specific Subject area	Density Functional Theory, Intermetallic compounds, Heusler Alloys
Data format	Excel, .dat
Type of data	Figures, Table, Collected data
Data collection	The first principal calculations were performed using Quantum Espresso [1] (Version 6.8) simulation package on X_2YZ Heusler alloys. The total energy of each alloy was calculated as a function of the calculated lattice parameter. A Self-Consistent Field (SCF) calculation followed by a non-SCF calculation were performed to get the Density of States (DOS) and projected Density of States (PDOS) of each of these alloys. Spin Polarization (P_F) was calculated by using the density of states (DOS) of spin-up and -down electrons at Fermi energy (E_F).
Data Source Location	Institution: The University of Alabama City, State: Tuscaloosa, Alabama Country: United States of America
Data accessibility	DOI:10.17632/by523ywzs9.3 Direct URL to data: https://data.mendeley.com/datasets/by523ywzs9/3

1. Value of the Data

- This dataset will provide fundamental information about 423 ternary Heusler alloys in their regular ($L2_1$) and inverse (XA) Heusler phases, for a total of 846 distinct alloys calculated. Structure, magnetic properties, and spin polarization values are provided as a launching point for future studies.
- This wide-scale database will serve as a valuable screening tool for identifying promising candidates and conducting thorough and comprehensive studies on ternary Heusler alloys.
- The dataset is also useful for machine learning studies of structure, phase stability, and electronic and magnetic properties of alloy systems.

2. Objective

Heusler alloys have attracted substantial attention within the research community due to their potential applications in fields such as spintronics [2] and thermo-electric devices [3]. Considerable focus is now being paid to identify novel candidates with advanced properties and their possible application in various fields. The enclosed comprehensive dataset of Heusler alloys, including structure properties and stability, magnetic structure and spin polarization, and electronic structure via density of states calculations, is valuable for researchers seeking to identify novel candidates and more quickly progress to subsequent in-depth theoretical and experimental exploration.

3. Data Description

Heusler compounds first attracted interest when Cu_2MnAl was discovered by German scientist Fritz Heusler in 1903 [4]. This remarkable face-centered cubic compound exhibited ferromagnetic properties although none of its constituent elements possessed inherent ferromagnetism. Motivated by this discovery, researchers worldwide have identified over a thousand Heusler alloys and their relatives within the past century and the quest for more continues to this day. To facilitate this quest, we have generated collections of X_2YZ Heusler alloys. This dataset stands out as one of the few comprehensive databases accessible for researchers in this field [5], offering a complementary source of data alongside the well-known Open Quantum Materials Datasets (OQMD) [6,7], Material Projects (MP) [8] and Automatic-FLOW for Materials Discovery (AFlow)

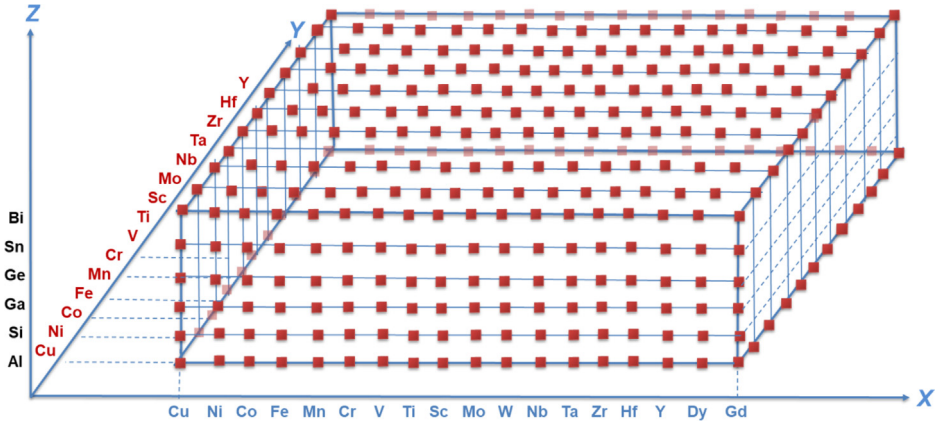

Fig. 1. Orthogonal element choice for density functional theory calculations.

[9]. Data on Materials Project (MP) are collected from two sources: (1) high-throughput calculations on supercomputing clusters; (2) academic community using MPContribs [10]. Data collected with (1) came from calculations performed using VASP [11], a well-reputed package that uses a full-potential method. However, self-consistent calculations (SCF) of many Heusler compounds and non-self-consistent calculations (NSCF) prior to DOS calculations were performed with a low k-point grid. Data for MP, OQMD and AFLOW were uploaded via Application Programming Interface (API) [12] from a supportive academic community comprise of many experienced researchers. However, the lack of a consistency in computation methods and parameters across over a thousand Heusler compounds makes it very difficult to create models of generalized behavior of Heuslers.

Moreover, MP, OQMD and AFLOW websites contain only a subset of Heusler compounds, many of which are included in our dataset. For example, the X_2VAl Heusler series featured in this manuscript, with X-sites choices Sc, Cu, Y, Nb, Mo, Hf, Ta and W, are not included in the MP website.

For our calculation, we have selected 18 D-block (including 2 rare earth) elements for X-site, most of these elements have also been used as Y-site and 6 main group elements as Z-site. Fig. 1 shows the orthogonal element choices for this work, sorted outward by atomic radius. Our calculations are based on a four atom-based face-centered cubic unit cell with 2 X-sites atoms and 1 Y and 1 Z site atoms, which represents one formula unit. Full Heusler structures consist of four interpenetrating face-centered cubic (fcc) sublattices positioned at (0, 0, 0), (1/4, 1/4, 1/4), (1/2, 1/2, 1/2), and (3/4, 3/4, 3/4). The sublattice sites (0, 0, 0) and (1/2, 1/2,1/2) are occupied by X atoms in a regular Heusler. The remaining sublattice sites (1/4, 1/4, 1/4) and (3/4,3/4, 3/4) are occupied by Y and Z elements respectively. 423 out of more than a thousand combinations have been calculated and presented in this dataset.

Table 1 summarizes the data collected on a series of X_2VAl (X = Sc, Ti, Cr, Mn, Fe, Co, Ni, Cu, Y, Zr, Nb. Mo, Hf, TA, W) full ($L2_1$) and inverse (XA) Heusler alloys. The total energy of the system can be conceptualized as the energy required to construct the system at absolute zero temperature by assembling single atoms of constituting elements. The calculations of density of states show that Y_2VAl, Zr_2VAl and Hf_2VAl are half metals in their inverse Heusler phases. Fig. 2 represents the total and atom-resolved density of states of X_2VAl alloy series in their $L2_1$ and XA phases.

The total density of states (DOS) and site-specific projected density of states (pDOS) of X_2VAl where X is one of the fifteen 3d elements presented in Table 1 are shown in Fig. 2. The $L2_1$ phases are displayed on the left and the *XA* phases are on the right side of the figure. The *X*-

Table 1
A list of lattice constant, energy, magnetic moment, and spin polarization of X_2VAl Heusler alloy in their regular ($L2_1$) and inverse (XA) Heusler phases.

Alloy	Phase	Lattice constant Å	Total energy (Ry)	Formation energy (eV/atom)	Magnetic moment per site, μ_B				Total magnetic moment, μ_B/f.u.	Spin polarization
					X_1	X_2	Y	Z		
Sc_2VAl	$L2_1$	6.7714	−567.4977	−0.17056	0.1673	0.1673	2.3806	−0.0714	3.23	5.23%
	XA	6.7489	−567.4663	−0.06391	0.0825	0.4922	2.4785	−0.0323	3.86	43.53%
Ti_2VAl	$L2_1$	6.3407	−620.9777	−0.19732	−0.0287	−0.0286	1.255	−0.0288	1.4	50.73%
	XA	6.3417	−620.9583	−0.13104	−0.3327	0.546	1.3756	−0.0156	1.96	70.68%
Cr_2VAl	$L2_1$	5.9524	−749.9959	−0.08087	1.6235	1.6236	−0.7581	−0.0033	2.71	43.51%
	XA	5.8951	−749.9738	−0.00545	0	0	0.0001	0	0	0.00%
Mn_2VAl	$L2_1$	5.9690	−826.6618	−0.37786	1.559	1.5583	−1	−0.026	2	25.23%
	XA	5.9015	−826.5904	−0.13511	2.5428	0.5262	0.7166	−0.0218	3.98	94.91%
Fe_2VAl	$L2_1$	5.7099	−912.2007	−0.69231	0	0	0.0001	0	0	0%
	XA	5.7741	−911.9523	0.15255	1.6024	1.8661	−0.2875	−0.0047	3.46	38.87%
Co_2VAl	$L2_1$	5.7594	−1007.034	−0.33519	−0.9443	−1.0985	−0.1302	0.0284	−2	25.23%
	XA	5.7988	−1006.981	−0.15652	0.8335	1.4253	−0.3906	−0.0079	1.76	67.46%
Ni_2VAl	$L2_1$	5.8068	−1111.966	−0.38555	−0.0069	0.0117	0.0041	−0.0004	0.01	6.09%
	XA	5.7966	−1111.937	−0.28638	0	0.0001	−0.0002	0	0	0%
Cu_2VAl	$L2_1$	5.9579	−1227.323	−0.07506	0.0224	0.0224	1.2526	−0.033	1.41	85.28%
	XA	5.9684	−1227.302	−0.00293	−0.0089	0.0455	1.3728	0.0362	1.63	69.85%
Y_2VAl	$L2_1$	7.2090	−818.7558	−0.08784	0.1014	0.1014	2.6523	−0.0912	3.3	37.36%
	XA	7.1527	−818.699	0.10459	0.0417	0.3554	2.78	−0.0385	4	100%
Zr_2VAl	$L2_1$	6.7401	−867.999	−0.16669	−0.0432	−0.0432	1.6678	−0.0454	1.75	40.55%
	XA	6.7089	−867.9606	−0.03418	−0.2972	0.1226	1.8524	−0.006	2	100%
Nb_2VAl	$L2_1$	6.4164	−922.0781	−0.05676	0	0	0	0	0	0%
	XA	6.4071	−922.0882	−0.09100	0	0	0	0	0	0%
Mo_2VAl	$L2_1$	6.2018	−981.3697	−0.03651	0.0003	0.0003	−0.0004	0	0	0%
	XA	6.2290	−981.3879	−0.09844	0.15	−0.1405	1.2328	0.0102	1.49	37.71%
Hf_2VAl	$L2_1$	6.6621	−1646.007	−0.14042	−0.022	−0.022	1.5501	−0.0477	1.68	24.50%
	XA	6.6488	−1645.964	0.00859	−0.1961	0.1817	1.6867	−0.0242	2	100%
Ta_2VAl	$L2_1$	6.4010	−1707.811	−0.03086	0.0055	−0.0055	0	0	0	0%
	XA	6.4143	−1707.816	−0.04591	−0.4263	−0.1553	0.8536	−0.0172	0.08	31.81%
W_2VAl	$L2_1$	6.2154	−1774.013	0.12564	0.0001	0.0001	−0.0001	0	0	0%
	XA	6.2514	−1774.051	−0.00202	0.1607	−0.0885	1.2538	0.016	1.63	0.00%

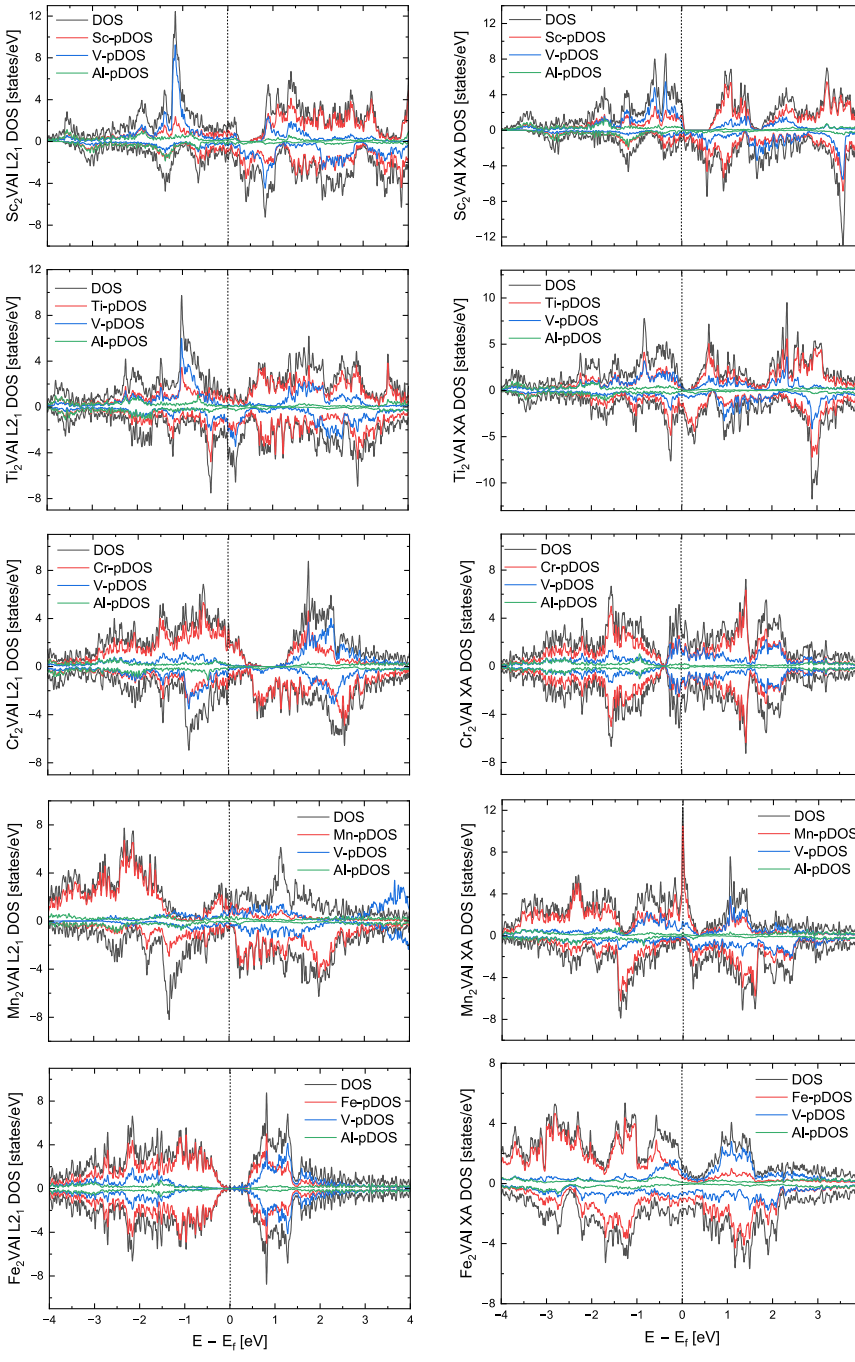

Fig. 2. Total density of states (DOS) and projected density of states (pDOS) of X_2VAl Heusler alloys (X = Sc, Ti, Cr, Mn, Fe, Co, Ni, Cu, Y, Zr, Nb, Mo, Hf, Ta, W).

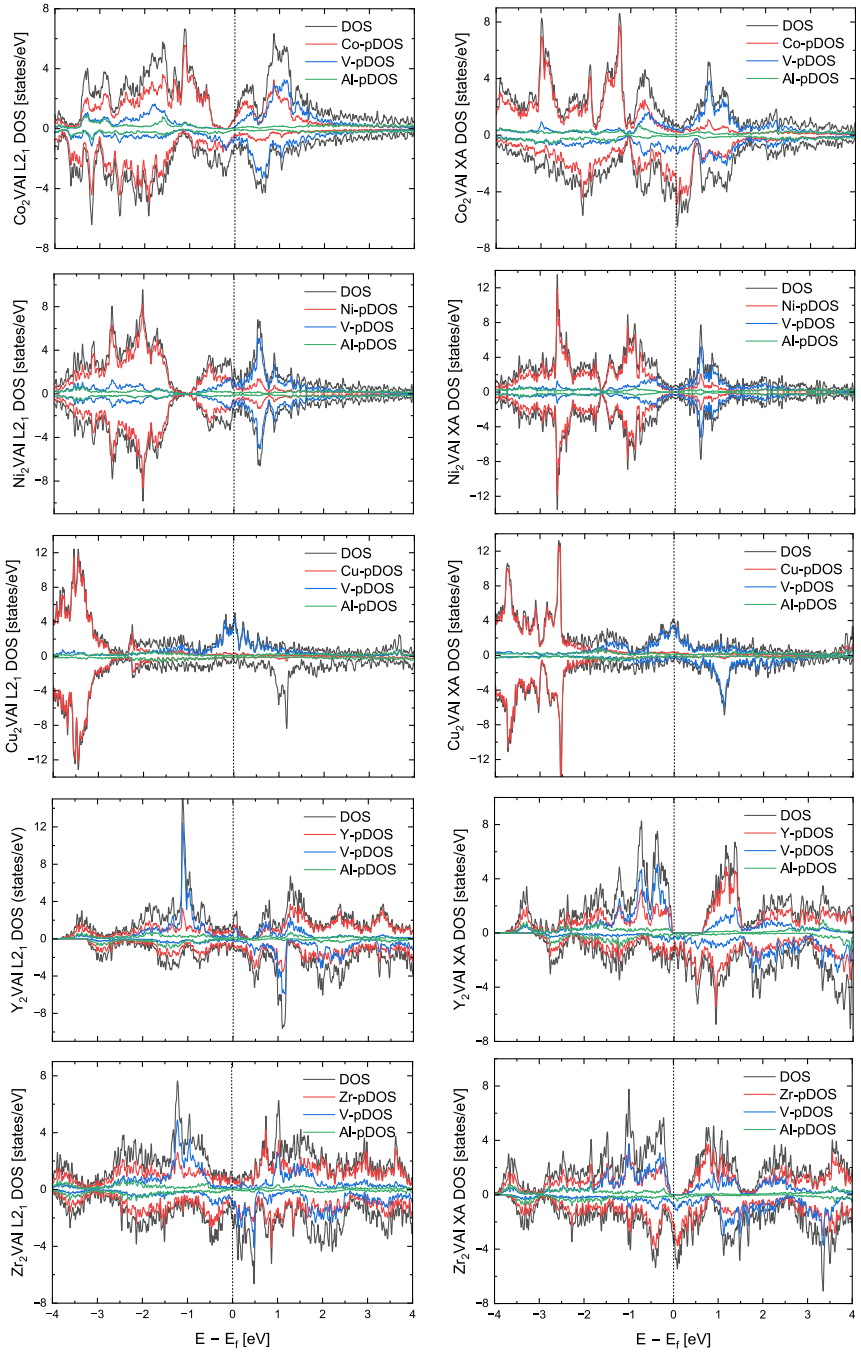

Fig. 2. Continued

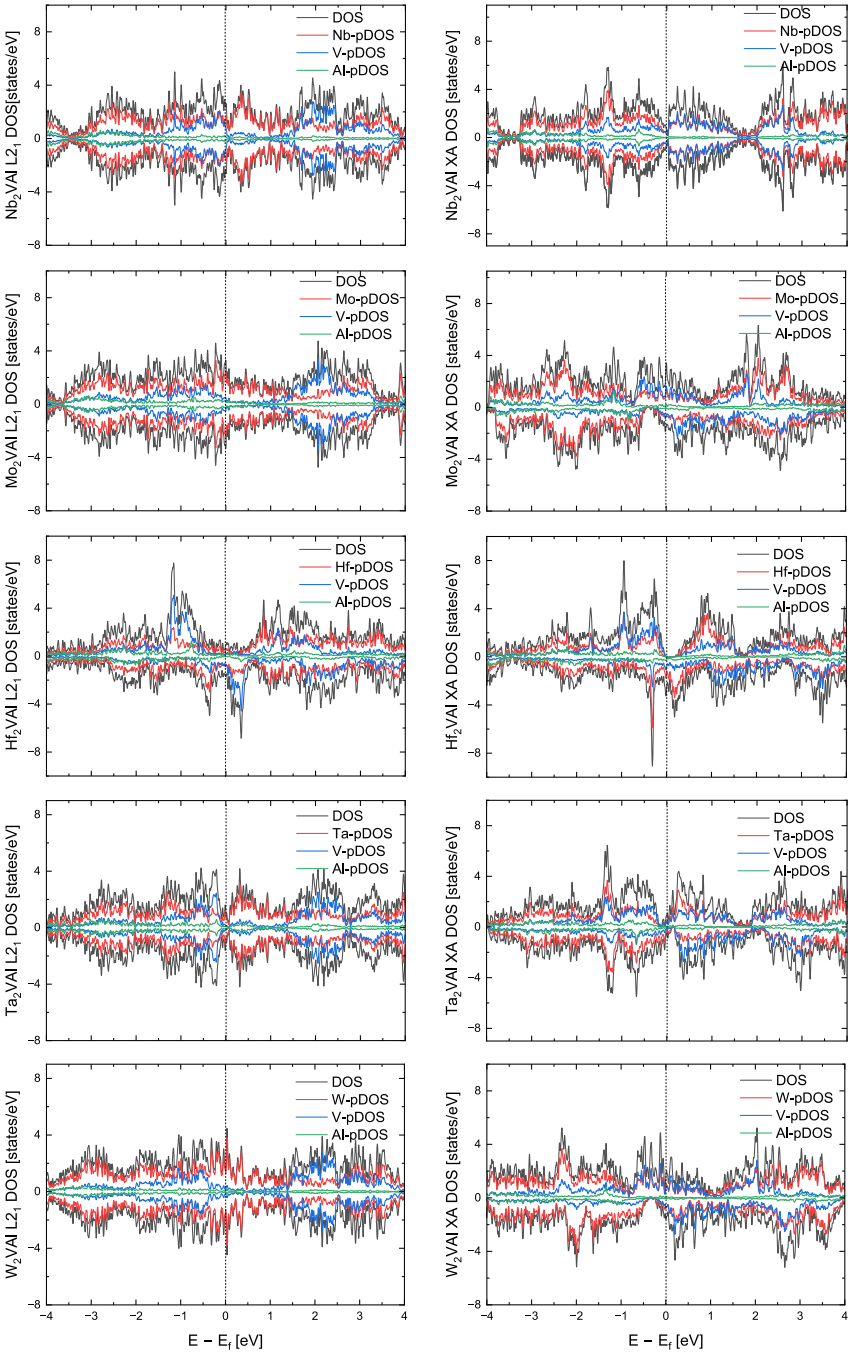

Fig. 2. Continued

pDOS is the sum of two *X* atoms in the alloy. The Fermi energy (E_F) is shifted to zero and is marked by a vertical line.

List of all included alloys, organized by Y-Z combination.

X_2FeAl: Sc_2FeAl, Ti_2FeAl, V_2FeAl, Cr_2FeAl, Mn_2FeAl, Co_2FeAl, Ni_2FeAl, Cu_2FeAl, Y_2FeAl, Zr_2FeAl, Nb_2FeAl, Mo_2FeAl, Hf_2FeAl, Ta_2FeAl, W_2FeAl, Dy_2FeAl, Gd_2FeAl

X_2FeGe: Sc_2FeGe, Ti_2FeGe, V_2FeGe, Cr_2FeGe, Mn_2FeGe, Co_2FeGe, Ni_2FeGe, Cu_2FeGe, Y_2FeGe, Zr_2FeGe, Nb_2FeGe, Hf_2FeGe, Ta_2FeGe, W_2FeGe, Dy_2FeGe, Gd_2FeGe

X_2FeSi: Sc_2FeSi, Ti_2FeSi, V_2FeSi, Cr_2FeSi, Mn_2FeSi, Co_2FeSi, Ni_2FeSi, Cu_2FeSi, Y_2FeSi, Zr_2FeSi, Hf_2FeSi, Ta_2FeSi, W_2FeSi, Gd_2FeSi, Dy_2FeSi

X_2FeGa: Sc_2FeGa, Ti_2FeGa, V_2FeGa, Cr_2FeGa, Mn_2FeGa, Ni_2FeGa, Cu_2FeGa, Y_2FeGa, Zr_2FeGa, Ta_2FeGa, Gd_2FeGa

X_2FeBi: Cr_2FeBi

X_2FeSn: Cr_2FeSn

X_2TiAl: Sc_2TiAl, V_2TiAl, Cr_2TiAl, Mn_2TiAl, Fe_2TiAl, Co_2TiAl, Ni_2TiAl, Cu_2TiAl, Y_2TiAl, Zr_2TiAl, Nb_2TiAl, Mo_2TiAl, Hf_2TiAl, Ta_2TiAl, W_2TiAl, Gd_2TiAl, Dy_2TiAl

X_2TiSi: Sc_2TiSi, V_2TiSi, Cr_2TiSi, Mn_2TiSi, Fe_2TiSi, Co_2TiSi, Ni_2TiSi, Cu_2TiSi, Y_2TiSi, Zr_2TiSi, Nb_2TiSi, Mo_2TiSi, Hf_2TiSi, Ta_2TiSi, W_2TiSi, Gd_2TiSi, Dy_2TiSi

X_2TiGe: Sc_2TiGe, V_2TiGe, Cr_2TiGe, Mn_2TiGe, Fe_2TiGe, Co_2TiGe, Ni_2TiGe, Cu_2TiGe, Y_2TiGe, Zr_2TiGe, Nb_2TiGe, Mo_2TiGe, Hf_2TiGe, Ta_2TiGe, W_2TiGe, Gd_2TiGe, Dy_2TiGe

X_2TiGa: V_2TiGa, Cr_2TiGa, Mn_2TiGa, Fe_2TiGa, Co_2TiGa, Ni_2TiGa, Cu_2TiGa, Zr_2TiGa, Ta_2TiGa, W_2TiGa, Gd_2TiGa, Dy_2TiGa

X_2TiSn: Co_2TiSn

X_2YAl: Sc_2YAl, Ti_2YAl, V_2YAl, Cr_2YAl, Mn_2YAl, Fe_2YAl, Co_2YAl, Ni_2YAl, Cu_2YAl, Zr_2YAl, Nb_2YAl, Hf_2YAl, Ta_2YAl, W_2YAl, Gd_2YAl, Dy_2YAl

X_2YGe: Sc_2YGe, Ti_2YGe, V_2YGe, Cr_2YGe, Mn_2YGe, Fe_2YGe, Co_2YGe, Ni_2YGe, Cu_2YGe, Zr_2YGe, Nb_2YGe, Hf_2YGe, Ta_2YGe, W_2YGe, Gd_2YGe, Dy_2YGe

X_2YSi: Sc_2YSi, Ti_2YSi, V_2YSi, Cr_2YSi, Mn_2YSi, Fe_2YSi, Co_2YSi, Ni_2YSi, Cu_2YSi Zr_2YSi, Nb_2YSi, Hf_2YSi, Ta_2YSi, W_2YSi, Gd_2YSi, Dy_2YSi

X_2YGa: Sc_2YGa, Ti_2YGa, Cr_2YGa, Mn_2YGa, Fe_2YGa, Co_2YGa, Ni_2YGa, Cu_2YGa, Zr_2YGa, Nb_2YGa, Hf_2YGa, Ta_2YGa, W_2YGa, Gd_2YGa

X_2YBi: Sc_2YBi, Ti_2YBi, V_2YBi, Cr_2YBi, Mn_2YBi, Fe_2YBi, Co_2YBi, Ni_2YBi, Cu_2YBi, Zr_2YBi, Nb_2YBi, Mo_2YBi, Hf_2YBi, Ta_2YBi, W_2YBi, Dy_2YBi, Gd_2YBi

X_2YSn: Sc_2YSn, Ti_2YSn, V_2YSn, Cr_2YSn, Mn_2YSn, Fe_2YSn, Co_2YSn, Ni_2YSn, Cu_2YSn, Zr_2YSn, Nb_2YSn, Mo_2YSn, Hf_2YSn, W_2YSn, Ta_2YSn

X_2CuAl: Sc_2CuAl, Cr_2CuAl, Mn_2CuAl, Fe_2CuAl, Co_2CuAl, Ni_2CuAl, Nb_2CuAl, Hf_2CuAl

X_2CuSi: Cr_2CuSi, Mn_2CuSi, Fe_2CuSi, Co_2CuSi, Ni_2CuSi

X_2CuGa: Sc_2CuGa, Ti_2CuGa, V_2CuGa, Cr_2CuGa, Mn_2CuGa, Fe_2CuGa, Co_2CuGa, Ni_2CuGa, Y_2CuGa, Zr_2CuGa, Nb_2CuGa, Mo_2CuGa, Hf_2CuGa, Ta_2CuGa, W_2CuGa, Dy_2CuGa, Gd_2CuGa

X_2CuGe: Sc_2CuGe, Ti_2CuGe, V_2CuGe, Cr_2CuGe, Mn_2CuGe, Fe_2CuGe, $Co_{22}CuGe$, Ni_2CuGe, Y_2CuGe, Zr_2CuGe, Nb_2CuGe, Mo_2CuGe, Hf_2CuGe, Ta_2CuGe, W_2CuGe, Dy_2CuGe, Gd_2CuGe

X_2CuSn: Mn_2CuSn

X_2CuSn: Mn_2CuBi

X_2CoAl: Sc_2CoAl, Ti_2CoAl, V_2CoAl, Cr_2CoAl, Mn_2CoAl, Fe_2CoAl, Ni_2CoAl, Cu_2CoAl, Y_2CoAl, Zr_2CoAl, Nb_2CoAl, Mo_2CoAl, Hf_2CoAl, Ta_2CoAl, W_2CoAl, Dy_2CoAl, Gd_2CoAl

X_2CoGa: Ti_2CoGa, Cr_2CoGa Fe_2CoGa, Ni_2CoGa, Gd_2CoGa, Dy_2CoGa

X_2CoGe: Cr_2CoGe, Mn_2CoGe, Fe_2CoGe, Ni_2CoGe, Gd_2CoGe, Dy_2CoGe

X_2CoSi: Cr_2CoSi, Mn_2CoSi, Fe_2CoSi, Ni_2CoSi, Cu_2CoSi, Mo_2CoSi, Gd_2CoSi, Dy_2CoSi

X_2CoBi: Cr_2CoBi, V_2CoBi

X_2CoSn: Cr_2CoSn, V_2CoSn

X_2MnAl: Sc_2MnAl, Cr_2MnAl, Fe_2MnAl, Co_2MnAl, Ni_2MnAl, Cu_2MnAl, Nb_2MnAl, Hf_2MnAl

X_2MnSi: Sc_2MnSi, Ti_2MnSi, V_2MnSi, Cr_2MnSi, Fe_2MnSi, Co_2MnSi, Ni_2MnSi, Cu_2MnSi

X_2MnGe: Sc_2MnGe, Cr_2MnGe, Co_2MnGe, Ni_2MnGe

X_2MnGa: Cr_2MnGa, Co_2MnGa, Ni_2MnGa

X_2MnSn: Co_2MnSn
X_2MnBi: Co_2MnBi
X_2CrAl: Sc_2CrAl, Fe_2CrAl, Mn_2CrAl, Ni_2CrAl, Nb_2CrAl, Hf_2CrAl, Dy_2CrAl, Gd_2CrAl
X_2CrSi: Fe_2CrSi, Ni_2CrSi, Gd_2CrSi, Dy_2CrSi
X_2CrGa: Ni_2CrGa, Gd_2CrGa, Dy_2CrGa
X_2CrGe: Ni_2CrGe, Gd_2CrGe, Dy_2CrGe
X_2NiAl: Sc_2NiAl, Cr_2NiAl, Cu_2NiAl, Nb_2NiAl, Hf_2NiAl, Ta_2NiAl
X_2NiSi: Cr_2NiSi
X_2NiGa: Cr_2NiGa
X_2NiGe: Cr_2NiGe
X_2NiBi: Cr_2NiBi
X_2NiSn: Cr_2NiSn
X_2ScAl: Cr_2ScAl, Fe_2ScAl, Ni_2ScAl, Cu_2ScAl, Nb_2ScAl, Hf_2ScAl
X_2ScSi: Cr_2ScSi, Fe_2ScSi, Ni_2ScSi
X_2ScGa: Cr_2ScGa, Fe_2ScGa, Ni_2ScGa
X_2ScGe: Cr_2ScGe, Fe_2ScGe, Ni_2ScGe
X_2ScSn: Co_2ScSn
X_2ZrAl: Cr_2ZrAl, Fe_2ZrAl, Ni_2ZrAl, Nb_2ZrAl
X_2ZrSi: Cr_2ZrSi, Fe_2ZrSi, Ni_2ZrSi
X_2ZrGa: Cr_2ZrGa, Fe_2ZrGa, Ni_2ZrGa
X_2ZrGe: Cr_2ZrGe, Fe_2ZrGe, Ni_2ZrGe
X_2VAl: Sc_2VAl, Ti_2VAl, Cr_2VAl, Mn_2VAl, Fe_2VAl, Co_2VAl, Ni_2VAl, Cu_2VAl, Y_2VAl, Zr_2VAl, Nb_2VAl, Mo_2VAl, Hf_2VAl, Ta_2VAl, W_2VAl
X_2VGa: Cr_2VGa, Fe_2VGa, Ni_2VGa
X_2VGe: Cr_2VGe, Fe_2VGe, Ni_2VGe
X_2VSi: Cr_2VSi, Fe_2VSi, Co_2VSi, Ni_2VSi
X_2NbAl: Fe_2NbAl, Y_2NbAl, Hf_2NbAl, Ta_2NbAl
X_2TaAl: Hf_2TaAl
X_2HfGe: Co_2HfGe
X_2HfAl: Co_2HfAl
X_2MoAl: Fe_2MoAl

4. Experimental Design, Materials and Methods

For the calculation, we have created four atom-based face-centered cubic unit cell and calculated its structural, electrical, and magnetic properties in both regular and inverse Heusler phases. It's worth mentioning here that inverse Heusler phase is a disordered structure of the full Heusler phase and can be obtained by swapping one of the *X*-site atoms with the *Y*-site. The density functional equations were solved using the plane-wave pseudopotential and projector-augmented-wave (PAW) approaches. The unknown exchange-correlation energy functional within the Khon-Sham equation was parametrized within the Perdew-Bruke-Ernzerhof (PBE) version of the generalized gradient approximation GGA. A Monkhorst-Pack special k-point mesh of 20 × 20 × 20, covering the irreducible part of the Brillouin zone was used for k-space integration. In our calculation, we didn't optimize cutoff energies, instead, we used very high cutoff to minimize error. The wave-function cutoff was set to 250 Ry for all alloy and element calculations and the kinetic energy cutoff for charge density for all cases were four times the wave-function cutoff i.e., 1000 Ry. (1 Ry = 13.6057 eV). The convergence of the total energy to a minimum value of 10–9 Ry was set as a criterion for the convergence of self-consistency loop and force convergence cutoff 10^{-5} Ry was used for all alloys and element calculations. The equilibrium lattice constant of these compounds was obtained by fitting the quadratic energy-volume graph, utilizing the Birch-Murnaghan equation of state.

$$E_T(V) = E_T(V_0) + \frac{B_0 V}{B_0'}\left[\frac{(V_0/V)^{B_0'}}{B_0' - 1} + 1\right] - \frac{V_0 B_0}{B_0' - 1} \quad (1)$$

Where E_T is the total energy for given volume V, B_0 is the bulk modulus at the equilibrium volume V_0 and B'_0 is the pressure derivative of the bulk modulus at the equilibrium volume V_0. The ground state lattice structure was obtained by relaxing the system using conjugate-gradient method which allows the cell shape and volume change freely until it finds the ground-state. All alloys were considered spin-polarized and a small non-zero starting magnetization value was set for all atomic types in the alloy. Pseudopotentials from Quantum Espresso PSLibrary (generated by A. Dal Corso) [13] were used in our calculations and are included in the Supplementary Material. The formation energy of the alloys is calculated by subtracting the energy corresponding to individual element from the calculated total energy (E_{total}) of the alloy. The value of E_{total} was obtained from the ground state self-consistent (SCF) calculations.

$$\Delta E_{form} = E_{total}^{X_2YZ} - 2 * E_{total}^{X} - E_{total}^{Y} - E_{total}^{Z} \tag{2}$$

For elemental calculations, the calculation steps and convergence parameters were the same as what we used for alloy calculations. The known ground state structure was used for all elements, e.g., simple hexagonal structure for Scandium, Hafnium, Zirconium, bcc structure for Chromium, Iron, fcc structure for Copper, Silicon, Aluminum, etc. A non-SCF calculation was performed after the self-consistent field (SCF) calculation to get the density of states (DOS) and projected density of states (pDOS) of each of these alloys. Spin Polarization (P_F) was calculated by using the density of states (DOS) at the Fermi energy in spin-up and -down states.

$$P_F = \left| \frac{n_{E_F}^{\uparrow} - n_{E_F}^{\downarrow}}{n_{E_F}^{\uparrow} + n_{E_F}^{\downarrow}} \right| \times 100\% \tag{3}$$

The calculations were performed without considering the effect of spin-orbit coupling.

Limitations

None.

Data Availability

Dataset on Density Functional Theory investigation of Ternary Heusler Alloys (Original data) (Mendeley Data)

CRediT Author Statement

Ridwan Nahar: Conceptualization, Investigation, Data curation, Writing – original draft; **Ka Ming Law:** Investigation, Data curation; **Thomas Roden:** Investigation, Data curation; **Michael Zengel:** Investigation, Data curation; **Justin Lewis:** Investigation, Data curation; **Sujan Budhathoki:** Investigation, Data curation; **Riley Nold:** Investigation, Data curation; **Harshil Avlani:** Investigation, Data curation; **Babajide Akintunde:** Investigation, Data curation; **Naomi Derksen:** Investigation, Data curation; **Adam J. Hauser:** Conceptualization, Validation, Data curation, Writing – review & editing, Project administration, Funding acquisition.

Ethics Statement

The proposed data does not involve any human subjects, animal experiments, or data collected from social media platforms.

Acknowledgement

The author gratefully acknowledges financial support from the National Science Foundation (NSF CAREER DMR-2047251)

Declaration of Competing Interest

The authors declare that they have no known competing financial interests or personal relationships that could have appeared to influence the work reported in this paper.

References

[1] P. Giannozzi, et al., QUANTUM ESPRESSO: a modular and open-source software project for quantum simulations of materials, J. Phys. Condens. Matter 21 (39) (2009) 395502.
[2] I. Galanakis, P.H. Dederichs, N. Papanikolaou, Slater-Pauling behavior and origin of the half-metallicity of the full-Heusler alloys, Phys. Rev. B (17) (2002) 66.
[3] B. Hinterleitner, et al., Thermoelectric performance of a metastable thin-film Heusler alloy, Nature 576 (7785) (2019) 85–90.
[4] Claudia Felser, G.H.F., Spintronics: from Materials to Device ⟨13:italic ⟩https://link.springer.com/book/10.1007/978-90-481-3832-6⟨/13:italic⟩.
[5] J. Ma, et al., Computational investigation of half-Heusler compounds for spintronics applications, Phys. Rev. B 95 (2) (2017).
[6] S. Kirklin, et al., The open quantum materials database (OQMD): assessing the accuracy of DFT formation energies, NPJ Comput. Mater. 1 (1) (2015).
[7] J.E. Saal, et al., Materials design and discovery with high-throughput density functional theory: the open quantum materials database (OQMD), JOM 65 (11) (2013) 1501–1509.
[8] A. Jain, et al., Commentary: the Materials Project: a materials genome approach to accelerating materials innovation, APL Mater. 1 (1) (2013).
[9] S. Curtarolo, et al., AFLOW: an automatic framework for high-throughput materials discovery, Comput. Mater. Sci. 58 (2012) 218–226.
[10] P. Huck, et al., User applications driven by the community contribution framework MPContribs in the Materials Project, Concurr. Comput.: Pract. Exp. 28 (7) (2015) 1982–1993.
[11] G. Kresse, J. Hafner, Ab initio molecular-dynamics simulation of the liquid-metal–amorphous-semiconductor transition in germanium, Phys. Rev. B 49 (20) (1994) 14251–14269.
[12] C.W. Andersen, et al., OPTIMADE, an API for exchanging materials data, Sci. Data 8 (1) (2021) 217.
[13] A. Dal Corso, Pseudopotentials periodic table: from H to Pu, Comput. Mater. Sci. 95 (2014) 337–350.